Articles
doi.org/10.1002/batt.202000040

Chemistry Europe
European Chemical Societies Publishing

Special Collection

Synthesis and Characteristics of Pyrrolidinium-Based Organic Ionic Plastic Crystals with Various Sulfonylamide Anions

Masahiro Yoshizawa-Fujita,*[a] Hiromasa Yamada,[a] Shun Yamaguchi,[a] Haijin Zhu,[b, c] Maria Forsyth,[b, c] Yuko Takeoka,[a] and Masahiro Rikukawa[a]

Organic ionic plastic crystals (OIPCs) have been studied as solid-state electrolytes owing to their desirable properties such as plasticity, non-flammability, and high ionic conductivity. However, the relationship between the ion structures and the properties of OIPCs are poorly understood. To supplement our previous work on the effects of the side chain structure of pyrrolidinium salts on their properties, this study examined the effects of the anion structure. For this purpose, five *N*,*N*-diethylpyrrolidinium ([C_2epyr]) salts with various sulfonylamide anions were synthesized. The [C_2epyr] salts with bis(fluorosulfonyl)amide ([FSA]) and bis(pentafluoroethanesulfonyl)amide ([BETA]) exhibited higher ionic conductivity values at room temperature than the other [C_2epyr] salts. The ^{1}H and ^{19}F solid-state NMR results indicated that the component ions in [C_2epyr][FSA] and [C_2epyr][BETA] exhibited high rotational mobility, even in the solid state. Thus, rotational mobility is likely important for achieving high ionic conductivity.

1. Introduction

Li-ion secondary batteries (LIBs) are today used in a wide range of applications from small electric devices to large-scale devices such as electric vehicles. However, the development and applications of LIBs have been restricted by safety issues associated with the high flammability, volatility, and leakage risk of conventional carbonate solvents. To improve the safety of LIBs, solid-state electrolytes have received much attention. Organic ionic plastic crystals (OIPCs) are organic salts that show a plastic crystal (PC) phase.[1] The PC phase is a kind of mesophase in which the ions are located on ordered sites in a periodic lattice but show local orientational and dynamic disorder. Thus, the ions in the PC phase show high mobility. If Li salts are added into OIPCs, the ion dynamics allow Li^+ transport,[2] and thereby, OIPCs can be used as solid-state electrolytes.[3–5] Recently, it has been reported that OIPCs can transport not only Li^+ but also Na^+,[6,7] H^+,[8–10] and I^-,[11,12] which allows them to be applied as electrolyte materials for Li-ion batteries, Na-ion batteries, fuel cells, and dye-sensitized solar cells. There has been a continual increase in the number of available OIPCs, the characteristics of which can be controlled by the combination of cation and anion species.[3,4] However, the relationship between the ionic structures and physicochemical properties of OIPCs are poorly understood. The ability to select OIPCs with suitable chemical structures for specific applications would aid in device development.

We have focused on pyrrolidinium-based OIPCs with bis(fluorosulfonyl)amide ([FSA]) anions because they are known to exhibit high chemical stability and a PC phase in a wide temperature range, including room temperature.[13] We previously reported the effect of the side chain structure of pyrrolidinium cations on the thermal and electrochemical properties.[14] The melting point (T_m) of pyrrolidinium-based OIPCs with [FSA] anions decreased as the side chain length of the cation increased. Symmetric pyrrolidinium cations with a longer alkyl chain (up to two carbons) showed a conductive PC phase in a wide temperature range and a higher ionic conductivity value. Yunis et al. also reported the synthesis and characterization of a symmetric pyrrolidinium cation combined with six different anions, and OIPCs were obtained. Pyrrolidinium-based OIPCs with [FSA] anion exhibited the highest ionic conductivity value of 1.9×10^{-5} S cm^{-1} at 30 °C.[15] In this study, the effect of the anion structure on the thermal properties, ionic conductivity, and ionic mobility were investigated. The *N*,*N*-diethylpyrrolidinium ([C_2epyr]) cation, which is symmetric, was combined with various sulfonylamide anions, which are known to have delocalized negative charges and to interact weakly with cations.[16] Such properties are suitable for the development of highly conductive electrolyte materials. Five OIPCs consisting of the [C_2epyr] cation and sulfonylamide anions with various side chain structures, bis(fluorosulfonyl)

[a] Prof. M. Yoshizawa-Fujita, H. Yamada, S. Yamaguchi, Prof. Y. Takeoka, Prof. M. Rikukawa
Department of Materials and Life Sciences
Sophia University
7-1 Kioi-cho, Chiyoda-ku, Tokyo 102-8554, Japan
E-mail: masahi-f@sophia.ac.jp
[b] Dr. H. Zhu, Prof. M. Forsyth
Institute for Frontier Materials
Deakin University
Geelong, Victoria 3216, Australia
[c] Dr. H. Zhu, Prof. M. Forsyth
ARC Centre of Excellence for Electromaterials Science
Deakin University
Burwood, Victoria 3125, Australia

Supporting information for this article is available on the WWW under https://doi.org/10.1002/batt.202000040

Special Collection An invited contribution to a Special Collection on Electrolytes for Electrochemical Energy Storage

amide ([FSA]), bis(trifluoromethanesulfonyl)amide ([TFSA]), bis(penta-fluoroethanesulfonyl)amide ([BETA]), bis(1,1,2,2,3,3,4,4,4-nonafluoro-1-butanesulfonyl)amide ([NFSA]), and 1,1,2,2,3,3-hexafluoro-propane-1,3-disulfonamide ([CFSA])) were synthesized (Figure 1), and their properties were investigated by means of thermal analysis, AC impedance spectroscopy, and solid-state NMR spectroscopy.

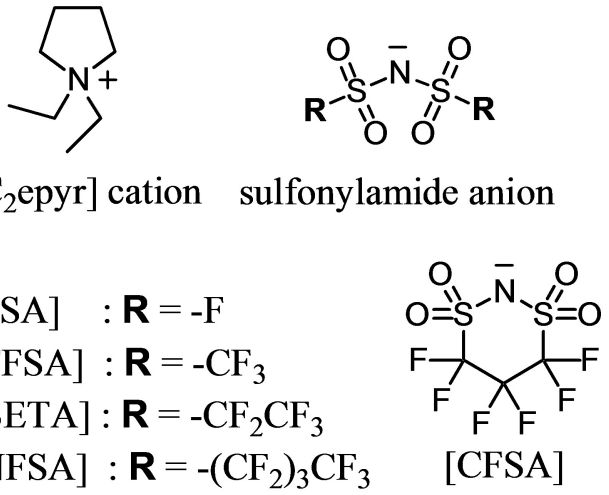

Figure 1. Chemical structures of [C_2epyr][FSA], [C_2epyr][TFSA], [C_2epyr][BETA], [C_2epyr][NFSA], and [C_2epyr][CFSA].

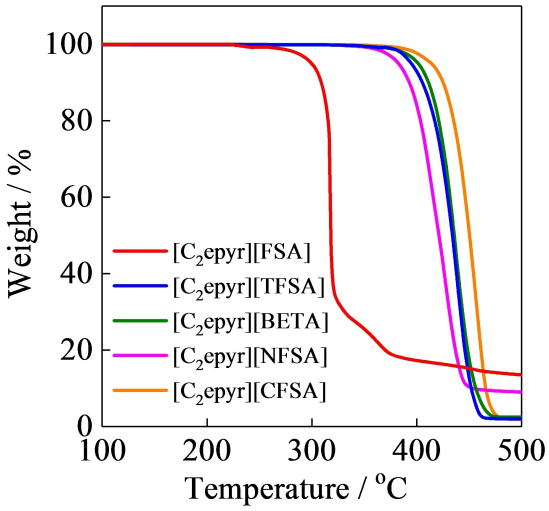

Figure 2. TGA curves of the pyrrolidinium-based organic salts with various sulfonylamide anions.

2. Results and Discussion

2.1. Thermal Properties

All the samples were obtained as white solids at room temperature. Analysing thermal stability and phase transition behaviour is an important to know the potential of organic salts as electrolyte materials. The thermal stabilities of the pyrrolidinium-based organic salts were evaluated by means of thermogravimetric analysis (TGA) under N_2 flow (200 mL min^{-1}), as shown in Figure 2. The 5% weight loss temperatures ($T_{d\text{-}5\%}$) of [C_2epyr][FSA], [C_2epyr][TFSA], [C_2epyr][BETA], [C_2epyr][NFSA], and [C_2epyr][CFSA] are 300, 395, 401, 382, and 414 °C, respectively. With the exception of [C_2epyr][FSA], all the samples exhibited a single-step weight loss process at approximately 400 °C, with almost all the weight lost in this decomposition step. The excellent thermal stabilities of these anions combined with pyrrolidinium cations are well known not only in ionic liquids[17] but also in OIPCs.[13,14,18] [C_2epyr][FSA] showed a significant weight loss resulting from decomposition at approximately 300 °C, and then a second thermal decomposition step. In the differential thermal analysis (DTA) measurement, [C_2epyr][FSA] showed a sharp exothermic peak at 300 °C, which should correspond to the thermal decomposition of the [FSA] anion. Because of the low thermal stability of fluorine–sulfur bonds, the [FSA] anion has a lower thermal stability than the other anions,[19,20] which have carbon–sulfur bonds. Thus, decomposition of [C_2epyr][FSA] occurred at a temperature approximately 100 °C lower than the $T_{d\text{-}5\%}$ values of the other four samples. However, the thermal resistance of [C_2epyr][FSA] was still acceptable for use in LIBs because the minimum thermal stability requirements for LIBs is 150 °C.

The 2nd differential scanning calorimetry (DSC) heating traces of the pyrrolidinium-based organic salts are shown in Figure 3. Table 1 summarizes their phase transition temperatures. One or more solid-solid phase transitions are observed for each sample. The solid phase at the highest temperature is labelled as Phase I, and those at lower temperatures are labelled successively as Phase II, III, etc. PCs are known to exist as anisotropic crystals at lower temperatures owing to restricted molecular motion. The unique properties of the PC

Table 1. Phase transition temperatures, ionic radius, and ionic radius ratio for the pyrrolidinium-based organic salts.

	$T_{V\text{–}IV}$[a] [°C]	$T_{IV\text{–}III}$[b] [°C]	$T_{III\text{–}II}$[c] [°C]	$T_{II\text{–}I}$[d] [°C]	T_m[e] [°C]	ΔS_f[f] [J K^{-1} mol^{-1}]	Ionic radius (r) [Å] Cation	Anion	Ionic radius ratio (ρ)
[C_2epyr][NFSA]	−26	−14	−2	8	92	16.2	3.31	4.13	0.801
[C_2epyr][FSA]	–	–	−125	−34	131	8.20		2.87	0.867
[C_2epyr][BETA]	–	–	−47	9	66	18.0		3.65	0.907
[C_2epyr][CFSA]	–	–	–	−25	258	12.3		3.35	0.988
[C_2epyr][TFSA]	−46	−29	7	32	95	22.9		3.30	0.997

[a] Phase V-to-IV transition temperature. [b] Phase IV-to-III transition temperature. [c] Phase III-to-II transition temperature. [d] Phase II-to-I transition temperature. [e] Melting point. [f] Entropy of fusion.

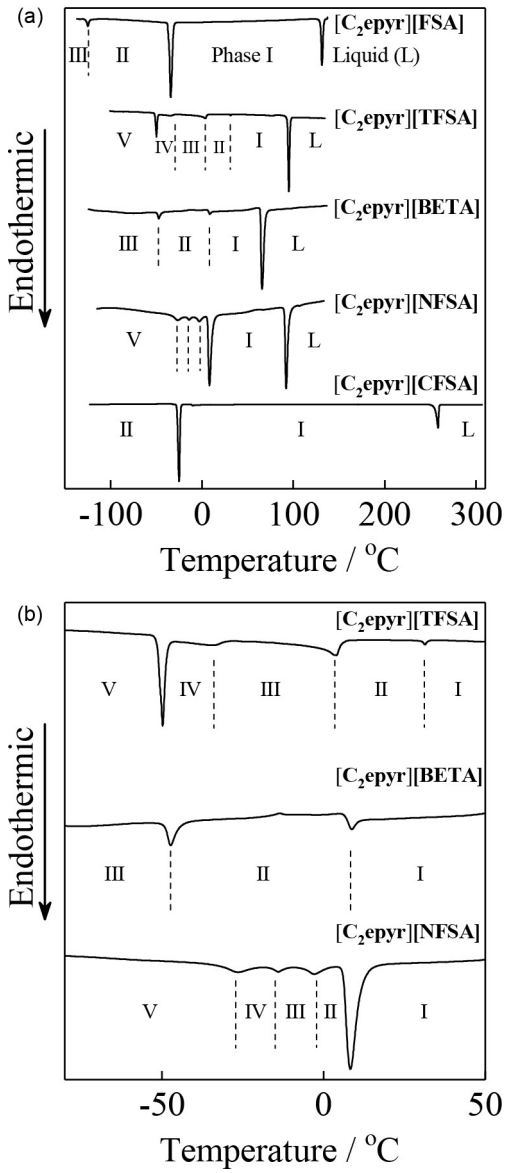

Figure 3. DSC traces (2nd heating) of a) the pyrrolidinium-based organic salts with various sulfonylamide anions. Enlarged DSC traces of b) [C_2epyr][TFSA], [C_2epyr][BETA], and [C_2epyr][NFSA].

phase, namely the orientational disorder and rotational mobility of molecules in the solid state, are generally obtained at a solid-solid phase transition that cause changes in the crystal system or the lattice constant.[21,22] The temperature of this interesting transition and the degree of rotational mobility in the PC phase depend on the chemical structure. The entropy change at the solid-solid phase transition and the T_m value provide important information about the solid-state phase. The final entropy of fusion (ΔS_f) of PCs is known to be relatively small owing to the orientational disorder of molecules in the PC phase. According to Timmermans' criterion for molecular compounds, the ΔS_f values of PCs should be smaller than 20 kJ K^{-1} mol^{-1}.[23] The ΔS_f values for [C_2epyr][FSA], [C_2epyr][TFSA], [C_2epyr][BETA], [C_2epyr][NFSA], and [C_2epyr][CFSA] are 8.20, 22.9, 18.0, 16.2, and 12.3 J K^{-1} mol^{-1}, respectively. Thus, with the exception of [C_2epyr][TFSA], all the samples are consistent with Timmermans' criterion, and these pyrrolidinium-based organic salts can be considered OIPCs. However, In the case of ionic compounds, owing to residual entropy based on electrostatic interactions, the ΔS_f values are likely to be larger than those of molecular compounds.[24–26] Hence, although the ΔS_f value of [C_2epyr][TFSA] was slightly larger than 20 J K^{-1} mol^{-1}, this salt could also be considered an OIPC.

For practical use in solid-state electrolytes, it is desirable to be in the PC phase at room temperature. All the samples, except for [C_2epyr][TFSA], were in Phase I, which shows a higher ionic mobility than the lower temperature phases (e.g. Phase II and Phase III), at room temperature. In contrast, [C_2epyr][TFSA] was in Phase II at 25 °C and the Phase II–I transition occurred at 32 °C. Furthermore, [C_2epyr][TFSA] melted at 95 °C with the largest ΔS_f value among the five samples. Of the four solid-solid phase transition peaks observed in the heating trace of [C_2epyr][TFSA], the initial one was relatively large but the other three were very small. [C_2epyr][FSA] melted at 131 °C with the smallest ΔS_f value among the five samples, possibly because the ionic orientation was very disordered in Phase I, which started at −34 °C (Phase II–I transition) with a large entropy change value (44.2 J K^{-1} mol^{-1}). The phase transition temperatures at 131 and −34 °C of [C_2epyr][FSA] has already been reported.[14,15] In this study, we found a new solid-solid phase transition at −125 °C with a small entropy change for [C_2epyr][FSA]. [C_2epyr][BETA] showed two solid-solid phase transitions at −47 and 9 °C with small entropy change values (1.0 and 1.4 J K^{-1} mol^{-1}, respectively). However, at T_m (66 °C), [C_2epyr][BETA] showed a relatively large entropy change value (18.0 J K^{-1} mol^{-1}). In the trace of [C_2epyr][NFSA], four solid-solid phase transitions were observed in succession, and the final peak was much larger than the others. [C_2epyr][NFSA] was in Phase I in the temperature range of 8–92 °C. [C_2epyr][CFSA] melted at 258 °C with the second smallest ΔS_f value (12.3 J K^{-1} mol^{-1}) among the five samples. The Phase I of [C_2epyr][CFSA] started at −25 °C with a large entropy change value (69.4 kJ K^{-1} mol^{-1}). Moriya et al. reported that OIPCs consisting of ammonium or pyrrolidinium cations and a [CFSA] anion exhibited the PC phase in a wide temperature range of more than 300 °C.[27] The PC phase of [C_2epyr][CFSA] also showed a remarkably wide temperature range, which included room temperature. Furthermore, [C_2epyr][FSA] and [C_2epyr][CFSA] showed similar simple phase transition behaviour.

The melting points of the pyrrolidinium-based organic salts decreased from 131 °C for [C_2epyr][FSA] to 66 °C for [C_2epyr][BETA] with increasing the carbon number of perfluoroalkyl chain in anion. Short side chain (F and C_nF_{n+1} (n is less than 2)) on anion decreased molecular symmetry and induced the distribution of molecular packing. The melting point of [C_2epyr][NFSA] ($n=4$) increased as compared with that of [C_2epyr][BETA]. Because perfluoroalkyl chain is immiscible with ionic part, the increase in melting point would attribute to the enhancement of molecular orientation which is based on the phase-separated layers of perfluoroalkyl chain and ionic part. Such phase separation has been used to synthesize liquid crystalline materials.[28]

2.2. Ionic Conductivity

The ionic conductivity of electrolyte materials is a key property for applying to rechargeable batteries. The ionic conductivity of OIPCs is greatly affected by the combination of cation and anion species. Recently, we proposed that the ionic radius ratio (ρ) values of cations and anions would be a good indicator to predict chemical structures of OIPCs, which show a higher ionic conductivity.[18] OIPCs with smaller ρ values tended to show higher ionic conductivities when ρ values were in the range of 0.8 and 1.0. But we still need to investigate the relationship between ionic conductivity and chemical structures of cation and anion species in detail. Here, the effect of sulfonylamide anions on ionic conductivity will be discussed.

Figure 4 shows Arrhenius plots of the ionic conductivities for the neat pyrrolidinium-based OIPC samples. The ionic conductivity of [C_2epyr][FSA] increased considerably at the solid-solid phase transition between −30 and −40 °C and reached 10^{-4} S cm^{-1} at 100 °C. The ionic conductivity value of [C_2epyr][BETA] increased ~10^3 times at the Phase II–I transition, despite the very small entropy change at this transition. [C_2epyr][BETA] exhibited high ionic conductivity values, which were comparable to those of [C_2epyr][FSA] just before melting. The ionic conductivity values of [C_2epyr][TFSA] and [C_2epyr][NFSA] were quite low at 25 °C ($<10^{-9}$ S cm^{-1}). However, at 90 °C, the ionic conductivity values of [C_2epyr][TFSA] and [C_2epyr][NFSA] significantly increased owing to melting. These behaviours agree well with the DSC results. The ionic conductivity of [C_2epyr][TFSA] did not increase rapidly at the solid-solid phase transition temperature of 32 °C, suggesting that this transition did not influence the ionic conduction of the component ions. The ionic conductivity values of the OIPCs at 25 °C decreased as follows: [C_2epyr][FSA] (9.6×10^{-6} S cm^{-1}) > [C_2epyr][BETA] (5.6×10^{-7} S cm^{-1}) > [C_2epyr][CFSA] (2.9×10^{-8} S cm^{-1}) > [C_2epyr][TFSA] (9.8×10^{-10} S cm^{-1}) > [C_2epyr][NFSA] (3.8×10^{-11} S cm^{-1}). The ionic conductivity values of [C_2epyr]-based salts with [BF_4] and [PF_6] anions, which are OIPCs, have also been reported by Yunis et al.[15] [C_2epyr][FSA] exhibited the highest ionic conductivity value at room temperature among various anions including [BF_4] and [PF_6] anions. Although [BETA] is a much larger anion than [FSA], both the corresponding OIPCs exhibited higher ionic conductivities than the other OIPCs used in this study. Thus, the mobility of the [C_2epyr] cation must also be important for achieving high ionic conductivity.

Table 1 summarizes the ionic radius (r) of the cation and anions and their ionic radius ratios (ρ) for the [C_2epyr]-based OIPCs. The optimised structures of OIPCs used in this study are shown in Figure S1. The r values were calculated according to the literature using the molecular modelling software program Winmostar.[18] Figure 5 shows the relationship between ionic conductivity value at 25 °C and ρ for [C_2epyr]-based salts with various sulfonylamide-anion species. This figure also includes the data for *N*-ethyl-*N*-methylpyrrolidinium ([C_2mpyr]) salts with various anion species for comparison.[18] Interestingly, OIPCs with smaller ρ values exhibited higher ionic conductivity values except for [C_2epyr][NFSA]. This tendency is consistent with that of [C_2mpyr]-based salts as can be seen in Figure 5. All the samples, which are [C_2epyr]- and [C_2mpyr]-based salts in Figure 5, would be categorized as the CsCl-type crystal structure based on the ρ values. A salt with a ρ value larger than 0.73 exhibits a CsCl-type crystal structure, whereas a salt with a ρ value between 0.41 and 0.73 exhibits a NaCl-type crystal structure.[29] As the ρ values approached the NaCl-type crystal structure, the ionic conductivity values were improved. However, [C_2epyr][NFSA] exhibited a quite low ionic conductivity value below 10^{-10} S cm^{-1} at 25 °C. We calculated the length of long-axis direction of each ion (the values are summarized in Table S1 in the Supporting information). The length of [NFSA] anion is 18.0 Å, which is the highest value among the ion species used in this study. The length of many ions is below

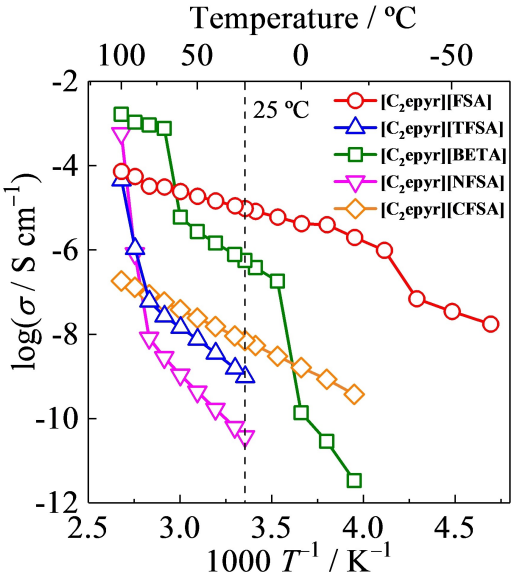

Figure 4. Arrhenius plots of ionic conductivities for the pyrrolidinium-based organic salts with various sulfonylamide anions.

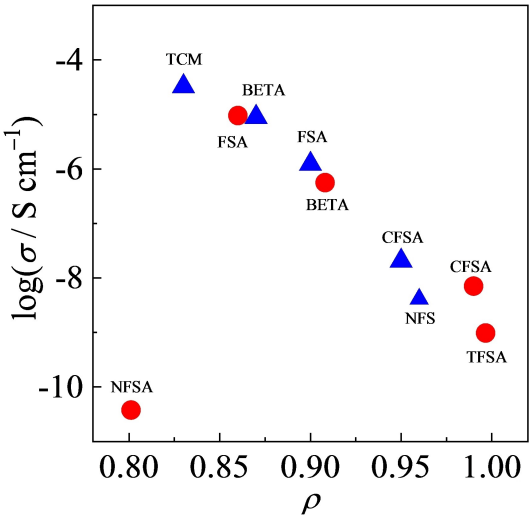

Figure 5. Relationship between ionic conductivity value at 25 °C and ρ for [C_2epyr]- (red circle) and [C_2mpyr]-based salts[18] (blue triangle) with various anion species. TCM: tricyanomethanide, NFS: nonafluorobutanesulfonate.

10 Å. The shape of [NFSA] anion may not be spherical even in the plastic crystal phase because the perfluoroalkyl chain length of [NFSA] anion would be too long to rotate at various angles in the crystal structure. For other four salts, since their shape would be close to a sphere to some extent in their plastic crystal phase due to the rotation of component ions, the ionic conductivity value and ρ exhibited a clear correlation. But further investigation is needed to precisely mention about the shape of ions in their crystal structure.

The temperature dependence of the ionic conductivities in the solid-state phases was well expressed by the Arrhenius equation. The activation energy values of ion conduction for [C_2epyr][FSA], [C_2epyr][TFSA], [C_2epyr][BETA], [C_2epyr][NFSA], and [C_2epyr][CFSA] in Phase I were calculated from the slopes of the Arrhenius plots as 22.7, 64.0, 51.4, 84.2, and 40.2 kJ mol^{-1}, respectively. Thus, the OIPCs that exhibited higher ionic conductivity values in the solid-state phases showed lower activation energy values of ion conduction in Phase I. The activation energy value of [C_2epyr][FSA] was almost the same with those of Li^+ conducting solid electrolytes, which show high ionic conductivity values of over 10^{-3} S cm^{-1} at room temperature.[30,31] Although the ionic conductivity value of [C_2epyr][FSA] is about 10^{-5} S cm^{-1} at room temperature, this value is greatly improved by doping a suitable amount of LiFSA.[14,32]

2.3. Ionic Mobility

To investigate the ionic mobility of the OIPCs, solid-state NMR measurements were conducted. Solid samples generally give broad NMR signals owing to dipole-dipole interactions and/or chemical shift anisotropy (CSA). However, the rotational motion of ions counteracts these effects and can narrow the NMR line width.[33–37] The dynamics of the [C_2epyr] cation and the sulfonylamide anions can be probed by analysing the ^{1}H and ^{19}F solid-state single-pulse NMR spectra, respectively. The ^{1}H solid-state NMR spectra of the five OIPCs at 20 °C are shown in Figure 6a. The signal shape changed depending on the sulfonylamide anion species, indicating that the side chain structure of the sulfonylamide anion affects the rotational dynamics of the [C_2epyr] cation in Phase I. Among the five OIPCs, [C_2epyr][FSA] exhibited the narrowest ^{1}H NMR signal at 20 °C, suggesting that the combination of the [C_2epyr] cation with the [FSA] anion shows the highest rotational mobility.

The full width at half maximum (FWHM) values of the ^{1}H NMR signals as a function of temperature are shown in Figure 6b. The corresponding ^{1}H solid-state NMR spectra of the five OIPCs at various temperatures are shown in the Supporting Information. Notably, [C_2epyr][FSA] exhibited low FWHM values (< 2 kHz) in the temperature range of 0–70 °C, even in the solid state. The temperature dependence was rather small in this temperature range (Phase I) because no phase transition occurred. Above 40 °C, [C_2epyr][BETA] also showed low FWHM values, similar to those of [C_2epyr][FSA]. As mentioned above, the T_m of [C_2epyr][BETA] was 66 °C and the Phase II–I transition occurred at 9 °C. After the Phase II–I transition, the FWHM

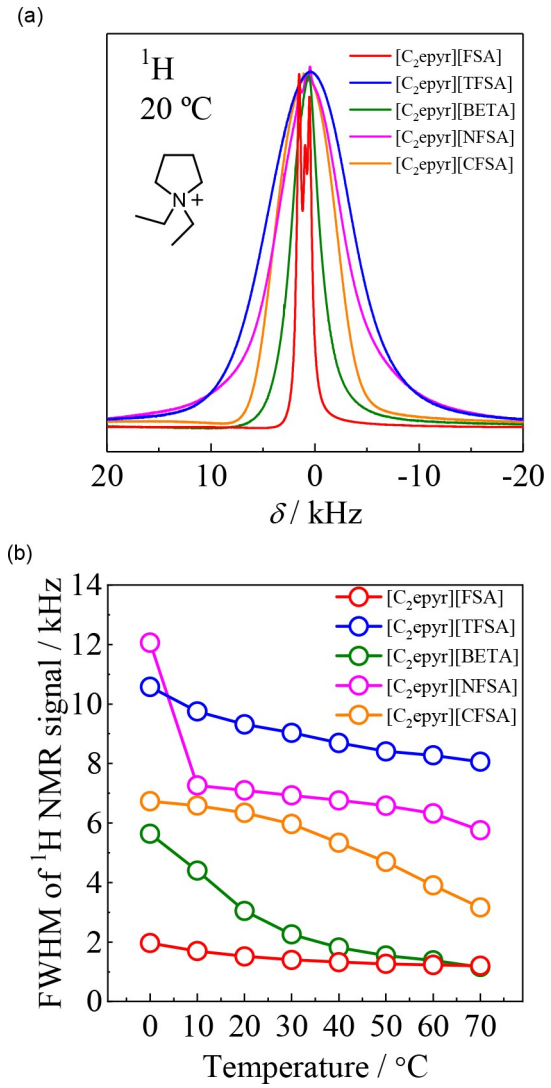

Figure 6. a) Solid-state ^{1}H NMR spectra of the pyrrolidinium-based organic salts with various sulfonylamide anions at 20 °C and b) FWHM of the ^{1}H NMR signals as a function of temperature.

values gradually decreased with increasing temperature. Interestingly, the FWHM values at 60 and 70 °C were almost the same, despite this salt being in the liquid state at 70 °C. This result suggested that the component ions of [C_2epyr][BETA] experienced liquid-like freedom in Phase I, which is a solid state. The FWHM values of the pyrrolidinium-based OIPCs at room temperature increase in the following order: [C_2epyr][FSA] < [C_2epyr][BETA] < [C_2epyr][CFSA] < [C_2epyr][NFSA] < [C_2epyr][TFSA]. This tendency is consistent with that observed for the ionic conductivity values, except for [C_2epyr][TFSA] and [C_2epyr][NFSA]. As the size and molecular weight of the [NFSA] anion are much larger than those of the [TFSA] anion, [C_2epyr][TFSA] is expected to exhibit higher ionic conductivity values than [C_2epyr][NFSA].

We also investigated the dynamics of the sulfonylamide anions using ^{19}F solid-state single-pulse NMR spectroscopy. The ^{19}F solid-state NMR spectra of the five OIPCs at each temperature in the range of 0–70 °C are shown in the Supporting

Information. The [FSA] and [BETA] anions clearly exhibited narrower ^{19}F signals than the [TFSA], [CFSA], and [NFSA] anions. This tendency is consistent with that observed for the ^{1}H NMR signals of the [C_2epyr] cation. Thus, the OIPCs that showed high ionic conductivity exhibited higher rotational mobilities for both the cation and anion species.

3. Conclusions

To advance the understanding of OIPCs, pyrrolidinium-based OIPCs with five different sulfonylamide anions were synthesized, and the effect of the sulfonylamide anion on the physicochemical properties was investigated. All the neat samples showed T_m values above room temperature and small ΔS_f values of less than 23 $J K^{-1} mol^{-1}$. The T_m values decreased with the increase in the perfluoroalkyl chain length of the sulfonylamide anions up to [BETA] anion, then [C_2epyr][NFSA] showed a higher T_m value. Furthermore, [C_2epyr][CFSA] with a cyclic anion showed the highest T_m value among the five pyrrolidinium salts. The ionic conductivity values of [C_2epyr][FSA] and [C_2epyr][BETA] were higher than those of the other three OIPCs. The dynamics of the constituent ions in each sample were evaluated by means of solid-state NMR measurements. The ^{1}H NMR signals of the [C_2epyr] cation for [C_2epyr][FSA] and [C_2epyr][BETA] were much narrower than those of the other three OIPCs owing to the rotational mobility of the cation. [C_2epyr][FSA] and [C_2epyr][BETA], which showed higher ionic conductivities, exhibited lower FWHM values in the solid phase for both the [C_2epyr] cation and the sulfonylamide anion. Thus, rotational mobility of the component ions is very important for achieving a high ionic conductivity in the PC phase. Positron annihilation lifetime spectroscopy (PALS) measurements were undertaken in order to determine the role of defect volume in conductivity by Pas et al.[38] A strong dependence of ionic conductivity on defect volume in each phase was shown, suggesting a defect mediated conduction mechanism. The anion structure would affect the defect volume in solid phases. The ionic conductivity of [C_2epyr][FSA] is higher than that of *N*-ethyl-*N*-methylpyrrolidinium bis(fluorosulfonyl)amide (1.23×10^{-6} $S cm^{-1}$ at 25 °C),[13] which has been successfully used in Li batteries.[39,40] [C_2epyr][FSA] will be used as electrolyte materials in Li batteries. The effect of Li-salt addition on electrochemical properties of [C_2epyr][FSA] will be reported elsewhere in detail.

Experimental Section

Materials

Lithium bis(fluorosulfonyl)amide (LiFSA) and lithium bis(trifluoromethanesulfonyl)amide were purchased from Kishida Chemical Co., Ltd. Lithium bis(pentafluoroethanesulfonyl)amide, lithium 1,1,2,2,3,3-hexafluoro-propane-1,3-disulfonamide, and *N*-ethylpyrrolidine (>97%) were purchased from Tokyo Chemical Industry Co., Ltd. Lithium bis(1,1,2,2,3,3,4,4,4-nonafluoro-1-butanesulfonyl) amide and iodoethane (>98.0%) were purchased from FUJIFILM Wako Pure Chemical Corporation. All solvents were purchased from Kanto Chemical Co., Inc. or FUJIFILM Wako Pure Chemical Corporation, and purified by the appropriate means if necessary.

Synthesis of *N*,*N*-Diethylpyrrolidinium Iodide ([C_2epyr]I)

[C_2epyr]I was synthesized from *N*-ethylpyrrolidine and iodoethane following a previously published route (yield: 70%).[14] ^{1}H NMR (400 MHz, CD_2Cl_2): δ = 3.75 (s, CH_2NCH_2), 3.55 (q, J=7.1 Hz, NCH_2CH_3), 2.26 (s, $CH_2CH_2CH_2CH_2$), 1.38 ppm (t, J=7.1 Hz, NCH_2CH_3); ^{13}C NMR (101 MHz, CD_2Cl_2): δ =63.5 (CH_2NCH_2), 56.0 (NCH_2CH_3), 23.2 ($CH_2CH_2CH_2CH_2$), 10.6 ppm (NCH_2CH_3); MS (FAB+): *m/z* 128.1 $[M]^+$, 383.0 $[2M+X]^+$; MS (FAB-): *m/z* 127.0 $[X]^-$, 382.0 $[2X+M]^-$; Anal. Calcd. for $C_8H_{18}NI$: C 37.7, H 7.11, N 5.49; found: C 37.7, H 7.13, N 5.49.

Synthesis of *N*,*N*-Diethylpyrrolidinium Bis(fluorosulfonyl) amide ([C_2epyr][FSA])

[C_2epyr][FSA] was synthesized from [C_2epyr]I and LiFSA following a previous route (yield: 76%).[14] ^{1}H NMR (400 MHz, CD_2Cl_2): δ =3.44 (s, CH_2NCH_2), 3.30 (q, J=7.2 Hz, NCH_2CH_3), 2.18 (s, $CH_2CH_2CH_2CH_2$), 1.32 ppm (t, J=7.2 Hz, NCH_2CH_3); ^{13}C NMR (101 MHz, CD_2Cl_2): δ =63.3 (CH_2NCH_2), 55.9 (NCH_2CH_3), 23.0 ($CH_2CH_2CH_2CH_2$), 9.6 ppm (NCH_2CH_3); ^{19}F NMR (376 MHz, CD_2Cl_2); δ =52.2 ppm (*SF*). MS (FAB+): *m/z* 128.2 $[M]^+$; MS (FAB-): *m/z* 180.0 $[X]^-$; Anal. Calcd. for $C_8H_{18}N_2O_4S_2F_2$: C 31.2, H 5.88, N 9.08, S 20.8; found: C 31.2, H 5.83, N 9.16, S 20.8.

Synthesis of *N*,*N*-Diethylpyrrolidinium Bis (trifluoromethanesulfonyl)amide ([C_2epyr][TFSA])

[C_2epyr][TFSA] was synthesized from [C_2epyr]I and lithium bis (trifluoromethanesulfonyl)amide in accordance with the procedure used to synthesize [C_2epyr][FSA] (yield: 89%). ^{1}H NMR (400 MHz, CD_2Cl_2): δ =3.45 (s, CH_2NCH_2), 3.30 (q, J=7.3 Hz, NCH_2CH_3), 2.21 (s, $CH_2CH_2CH_2CH_2$), 1.35 ppm (t, J=7.3 Hz, NCH_2CH_3); ^{13}C NMR (101 MHz, CD_2Cl_2): δ =63.6 (CH_2NCH_2), 56.1 (NCH_2CH_3), 23.1 ($CH_2CH_2CH_2CH_2$), 9.8 ppm (NCH_2CH_3); ^{19}F NMR (376 MHz, CD_2Cl_2): δ =-79.5 ppm (CF_3); MS (FAB+): *m/z* 128.2 $[M]^+$; MS (FAB-): *m/z* 279.9 $[X]^-$; Anal. Calcd. for $C_{10}H_{18}N_2O_4S_2F_6$: C 29.4, H 4.44, N 6.86, S 15.7; found: C 29.5, H 4.35, N 6.65, S 15.7.

Synthesis of *N*,*N*-Diethylpyrrolidinium Bis (pentafluoroethanesulfonyl)amide ([C_2epyr][BETA])

[C_2epyr][BETA] was synthesized from [C_2epyr]I and lithium bis (pentafluoroethanesulfonyl)amide in accordance with the procedure used to synthesize [C_2epyr][FSA] (yield: 85%). ^{1}H NMR (400 MHz, CD_2Cl_2): δ =3.43 (s, CH_2NCH_2), 3.29 (q, J=7.3 Hz, NCH_2CH_3), 2.18 (s, $CH_2CH_2CH_2CH_2$), 1.32 ppm (t, J=7.3 Hz, NCH_2CH_3); ^{13}C NMR (101 MHz, CD_2Cl_2): δ =119.5 (tq, J=133.3, 1142.8 Hz, CF_2CF_3), 113.2 (qt, J=152.8, 1176.4 Hz, CF_2CF_3), 63.5 (CH_2NCH_2), 56.1 (NCH_2CH_3), 23.1 ($CH_2CH_2CH_2CH_2$), 9.7 ppm (NCH_2CH_3); ^{19}F NMR (376 MHz, CD_2Cl_2): δ =-79.6 (CF_2CF_3), −117.7 ppm (CF_2CF_3); MS (FAB+): *m/z* 128.2 $[M]^+$, 636.0 $[2M+X]^+$; MS (FAB-): *m/z* 379.9 $[X]^-$, 887.8 $[2X+M]^-$; Anal. Calcd. for $C_{12}H_{18}N_2O_4S_2F_{10}$: C 28.4, H 3.57, N 5.51, S 12.6; found: C 28.4, H 3.36, N 5.48, S 13.3.

Synthesis of *N*,*N*-Diethylpyrrolidinium Bis (1,1,2,2,3,3,4,4,4-nonafluoro-1-butanesulfonyl)amide ([C_2epyr][NFSA])

[C_2epyr][NFSA] was synthesized from [C_2epyr]I and lithium bis (1,1,2,2,3,3,4,4,4-nonafluoro-1-butanesulfonyl)amide in accordance with the procedure used to synthesize [C_2epyr][FSA] (yield: 86%). ^{1}H NMR (400 MHz, CD_2Cl_2): δ = 3.45 (s, CH_2NCH_2), 3.30 (q, J = 7.2 Hz, NCH_2CH_3), 2.18 (s, $CH_2CH_2CH_2CH_2$), 1.32 ppm (t, J = 7.2 Hz, NCH_2CH_3); ^{13}C NMR(101 MHz, CD_2Cl_2): δ = 123.6–107.2 ($CF_2CF_2CF_2CF_3$), 62.6 (CH_2NCH_2), 56.2 (NCH_2CH_3), 23.2 ($CH_2CH_2CH_2CH_2$), 9.7 ppm (NCH_2CH_3); ^{19}F NMR (376 MHz, CD_2Cl_2): δ = -81.5 ($CF_2CF_2CF_2CF_3$), −113.3 ($CF_2CF_2CF_2CF_3$), −121.5 ($CF_2CF_2CF_2CF_3$), −126.4 ppm ($CF_2CF_2CF_2CF_3$); MS (FAB+): *m/z* 128.2 $[M]^+$, 836.1 $[2M+X]^+$; MS (FAB-): *m/z* 580.0 $[X]^-$, 1288.1 $[2X+M]^-$; Anal. Calcd. for $C_{16}H_{18}N_2O_4S_2F_{18}$: C 27.1, H 2.56, N 3.95, S 9.05; found: C 27.2, H 2.24, N 3.93, S 9.53.

Synthesis of *N*,*N*-Diethylpyrrolidinium 1,1,2,2,3,3-Hexafluoropropane-1,3-disulfonamide ([C_2epyr][CFSA])

[C_2epyr][CFSA] was synthesized from [C_2epyr]I and lithium 1,1,2,2,3,3-hexafluoropropane-1,3-disulfonamide in accordance with the procedure used to synthesize [C_2epyr][FSA] (yield: 92%). ^{1}H NMR (400 MHz, CD_2Cl_2): δ = 3.44 (s, CH_2NCH_2), 3.30 (q, J = 7.2 Hz, NCH_2CH_3), 2.20 (s, $CH_2CH_2CH_2CH_2$), 1.34 ppm (t, J = 7.2 Hz, NCH_2CH_3); ^{13}C NMR (101 MHz, CD_2Cl_2): δ = 114.3 (tt, J = 101.1, 1188.0 Hz, $CF_2CF_2CF_2$), 111.0 (quin t, J = 101.7, 1089.1 Hz, $CF_2CF_2CF_2$), 62.6 (CH_2NCH_2), 56.1 (NCH_2CH_3), 23.1 ($CH_2CH_2CH_2CH_2$), 9.8 ppm (NCH_2CH_3); ^{19}F NMR (376 MHz, CD_2Cl_2): δ = -120.0 ($CF_2CF_2CF_2$), −126.5 ppm ($CF_2CF_2CF_2$); MS (FAB+): *m/z* 128.2 $[M]^+$; MS (FAB-): *m/z* 292.0 $[X]^-$; Anal. Calcd. for $C_{11}H_{18}N_2O_4S_2F_6$: C 31.4, H 4.32, N 6.66, S 15.3; found: C 31.6, H 4.29, N 6.69, S 15.4.

Characterization

^{1}H, ^{13}C, and ^{19}F solution NMR spectra were recorded on a Bruker AVANCE III HD 400 MHz spectrometer at room temperature. The signals were referenced against tetramethylsilane (for ^{1}H and ^{13}C NMR) and trifluoroacetic acid (for ^{19}F NMR) as internal standards. Fast atom bombardment mass spectroscopy (FAB-MS) was conducted using a JMS-T100LC system. Elemental analyses were carried out with a PerkinElmer PE 2400-II unit. TGA and DTA were performed on a TG-DTA7200 instrument under a N_2 atmosphere at a scanning rate of 10 °C min^{-1}. DSC was performed on a DSC7020 instrument under a N_2 atmosphere at a scanning rate of 5 °C min^{-1}.

Ionic conductivity measurements were carried out in stainless cells (TYS-00DM01, Toyo System Co., Ltd.). The cells were fabricated in an Ar-filled glovebox (dew point temperature < −80 °C, O_2 concentration < 1 ppm). The Pt electrodes were polished with 1.0, 0.3, and 0.05 μm Al_2O_3 powders. AC impedance spectroscopy measurements (VSP-300; BioLogic) were conducted over a frequency range of 7 MHz to 0.1 Hz (applied voltage: 10 mV). The temperature was controlled using a constant temperature oven (SU262, Espec Corp.).

Solid-state ^{1}H and ^{19}F single-pulse NMR experiments were performed on a Bruker AVANCE III 500 MHz spectrometer with a 4 mm double-resonance magic-angle spinning probe. The ^{1}H and ^{19}F NMR spectra were recorded at various temperatures (0–70 °C) without spinning. The 90° pulse lengths were 4.0 μs for both nuclei, and the recycle delays were 5 and 10 s in the ^{1}H and ^{19}F NMR experiments, respectively.

Acknowledgements

This work was supported by JSPS KAKENHI Grant Number 19K05604, JSPS Bilateral Program Grant number JPJSBP120199977, and a Sophia University Special Grant for Academic Research.

Conflict of Interest

The authors declare no conflict of interest.

Keywords: organic ionic plastic crystals · solid-state electrolytes · mesophases · sulfonylamide anions · NMR spectroscopy

[1] D. R. MacFarlane, M. Forsyth, *Adv. Mater.* **2001**, *13*, 957–966.
[2] D. R. MacFarlane, J. Huang, M. Forsyth, *Nature* **1999**, *402*, 792–794.
[3] J. M. Pringle, P. C. Howlett, D. R. MacFarlane, M. Forsyth, *J. Mater. Chem.* **2010**, *20*, 2056–2062.
[4] J. M. Pringle, *Phys. Chem. Chem. Phys.* **2013**, *15*, 1339–1351.
[5] Z.-B. Zhou, H. Matsumoto, *Electrochem. Commun.* **2007**, *9*, 1017–1022.
[6] M. Forsyth, T. Chimdi, A. Seeber, D. Gunzelmann, P. C. Howlett, *J. Mater. Chem. A* **2014**, *2*, 3993–4003.
[7] F. Makhlooghiazad, J. Guazzagaloppa, L. A. O'Dell, R. Yunis, A. Basile, P. C. Howlett, M. Forsyth, *Phys. Chem. Chem. Phys.* **2018**, *20*, 4721–4731.
[8] M. Yoshizawa-Fujita, K. Fujita, M. Forsyth, D. R. MacFarlane, *Electrochem. Commun.* **2007**, *9*, 1202–1205.
[9] U. A. Rana, P. M. Bayley, R. Vijayaraghavan, P. C. Howlett, D. R. MacFarlane, M. Forsyth, *Phys. Chem. Chem. Phys.* **2010**, *12*, 11921–11928.
[10] U. A. Rana, R. Vijayaraghavan, D. R. MacFarlane, M. Forsyth, *Chem. Commun.* **2011**, *47*, 6401–6403.
[11] Q. Li, J. Zhao, B. Sun, B. Lin, L. Qiu, Y. Zhang, X. Chen, J. Lu, F. Yan, *Adv. Mater.* **2012**, *24*, 945–950.
[12] Q. Li, X. Chen, J. Zhao, L. Qiu, Y. Zhang, B. Sun, F. Yan, *J. Mater. Chem.* **2012**, *22*, 6674–6679.
[13] M. Yoshizawa-Fujita, E. Kishi, M. Suematsu, T. Takekawa, M. Rikukawa, *Chem. Lett.* **2014**, *43*, 1909–1911.
[14] H. Yamada, Y. Miyachi, Y. Takeoka, M. Rikukawa, M. Yoshizawa-Fujita, *Electrochim. Acta* **2019**, *303*, 293–298.
[15] R. Yunis, T. W. Newbegin, A. F. Hollenkamp, J. M. Pringle, *Mater. Chem. Front.* **2018**, *2*, 1207–1214.
[16] P. Bonhôte, A.-P. Dias, M. Armand, N. Papageorgiou, K. Kalyanasundaram, M. Grätzel, *Inorg. Chem.* **1996**, *35*, 1168–1178.
[17] M. Yoshizawa-Fujita, K. Johansson, P. Newman, D. R. MacFarlane, M. Forsyth, *Tetrahedron Lett.* **2006**, *47*, 2755–2758.
[18] S. Yamaguchi, H. Yamada, Y. Takeoka, M. Rikukawa, M. Yoshizawa-Fujita, *New J. Chem.* **2019**, *43*, 4008–4012.
[19] J. Huang, A. F. Hollenkamp, *J. Phys. Chem. C* **2010**, *114*, 21840–21847.
[20] J. Reiter, S. Jeremias, E. Paillard, M. Winter, S. Passerini, *Phys. Chem. Chem. Phys.* **2013**, *15*, 2565–2571.
[21] T. Enomoto, S. Kanematsu, K. Matsumoto, R. Hagiwara, *Phys. Chem. Chem. Phys.* **2011**, *13*, 12536–12544.
[22] K. Matsumoto, U. Harinaga, R. Tanaka, A. Koyama, R. Hagiwara, K. Tsunashima, *Phys. Chem. Chem. Phys.* **2014**, *16*, 23616–23626.
[23] J. Timmermans, *J. Phys. Chem. Solids* **1961**, *18*, 1–8.
[24] A. Xenopoulos, J. Cheng, M. Yasuniwa, B. Wunderlich, *Mol. Cryst. Liq. Cryst.* **1992**, *214*, 63–79.
[25] J. Sun, D. R. MacFarlane, *Solid State Ionics* **2002**, *148*, 145–151.
[26] R. Asayama, J. Kawamura, T. Hattori, *Chem. Phys. Lett.* **2005**, *414*, 87–91.
[27] M. Moriya, T. Watanabe, W. Sakamoto, T. Yogo, *RSC Adv.* **2012**, *2*, 8502–8507.
[28] T. Mukai, M. Yoshio, T. Kato, H. Ohno, *Chem. Lett.* **2005**, *34*, 442–443.
[29] P. Atkins, T. Overton, J. Rourke, M. Weller, F. Armstrong, *Shriver and Atkins' Inorganic Chemistry*, Oxford University Press, Oxford, 5th edn, **2010**.

[30] N. Kamaya, K. Homma, Y. Yamakawa, M. Hirayama, R. Kanno, M. Yonemura, T. Kamiyama, Y. Kato, S. Hama, K. Kawamoto, A. Mitsui, *Nat. Mater.* **2011**, *10*, 682–686.
[31] G. Sahu, E. Rangasamy, J. Li, Y. Chen, K. An, N. Dudney, C. Liang, *J. Mater. Chem. A* **2014**, *2*, 10396–10403.
[32] D. Al-Masri, R. Yunis, A. F. Hollenkamp, J. M. Pringle, *Chem. Commun.* **2018**, *54*, 3660–3663.
[33] J. M. Pringle, J. Adebahr, D. R. MacFarlane, M. Forsyth, *Phys. Chem. Chem. Phys.* **2010**, *12*, 7234–7240.
[34] L. Jin, K. M. Nairn, C. M. Forsyth, A. J. Seeber, D. R. MacFarlane, P. C. Howlett, M. Forsyth, J. M. Pringle, *J. Am. Chem. Soc.* **2012**, *134*, 9688–9697.
[35] U. A. Rana, R. Vijayaraghavan, C. M. Doherty, A. Chandra, J. Efthimiadis, A. J. Hill, D. R. MacFarlane, M. Forsyth, *J. Phys. Chem. C* **2013**, *117*, 5532–5543.
[36] M. Matsuki, T. Yamada, S. Dekura, H. Kitagawa, N. Kimizuka, *Chem. Lett.* **2018**, *47*, 497–499.
[37] Y. Yamada, E. Kashimoto, H. Honda, *Bull. Chem. Soc. Jpn.* **2019**, *92*, 1289–1298.
[38] S. J. Pas, J. Huang, M. Forsyth, D. R. MacFarlane, A. J. Hill, *J. Chem. Phys.* **2005**, *122*, 064704.
[39] X. Wang, H. Zhu, G. W. Greene, Y. Zhou, M. Yoshizawa-Fujita, Y. Miyachi, M. Armand, M. Forsyth, J. M. Pringle, P. C. Howlett, *Adv. Mater. Technol.* **2017**, 1700046.
[40] Y. Zhou, X. Wang, H. Zhu, M. Yoshizawa-Fujita, Y. Miyachi, M. Armand, M. Forsyth, G. W. Greene, J. M. Pringle, P. C. Howlett, *ChemSusChem* **2017**, *10*, 3135–3145.

Manuscript received: February 24, 2020
Revised manuscript received: April 6, 2020
Accepted manuscript online: April 24, 2020
Version of record online: May 13, 2020